Active Reaction Sites and Oxygen Reduction Kinetics on $La_{1-x}Sr_xMnO_{3+\delta}$ (x=0.1-0.4)/YSZ (Yttria-Stabilized Zirconia) Electrodes for Solid Oxide Fuel Cells

Hee Y. Lee, Woo S. Cho, and Seung Mo Oh*

Department of Chemical Technology, College of Engineering, Seoul National University, Seoul 151-742, Korea
Received February 12, 1998

Active reaction sites and electrochemical O_2 reduction kinetics on $La_{1-x}Sr_xMnO_{3+\delta}$ (x=0.1-0.4)/YSZ (yttria-stabilized zirconia) electrodes are investigated in the temperature range of 700-900 °C at $P_{O_2}=10^{-3}$-0.21 atm. Results of the steady-state polarization measurements, which are formulated into the Butler-Volmer formalism to extract transfer coefficient values, lead us to conclude that the two-electron charge transfer step to atomically adsorbed oxygen is rate-limiting. The same conclusion is drawn from the P_{O_2}-dependent ac impedance measurements, where the exponent m in the relationship of I_0 (exchange current density) $\propto P_{O_2}^m$ is analyzed. Chemical analysis is performed on the quenched Mn perovskites to estimate their oxygen stoichiometry factors (δ) at the operating temperature (700-900 °C). Here, the observed δ turns out to become smaller as both the Sr-doping contents (x) and the measured temperature increase. A comparison between the δ values and cathodic activity of Mn perovskites reveals that the cathodic transfer coefficients (α_c) for oxygen reduction reaction are inversely proportional to δ whereas the anodic ones (α_a) show the opposite trend, reflecting that the surface oxygen vacancies on Mn perovskites actively participate in the O_2 reduction reaction. Among the samples of x= 0.1-0.4, the manganite with x=0.4 exhibits the smallest δ value (even negative), and consistently this electrode shows the highest α_c and the best cathodic activity for the oxygen reduction reaction.

Introduction

Sr-doped lanthanum manganites ($La_{1-x}Sr_xMnO_{3+\delta}$) are considered as one of the promising cathode materials for solid oxide fuel cell systems.[1,2] Even though many theoretical and experimental results have been reported on this material, there still remain controversies on both the nature of active reaction sites for the O_2 reduction reaction and the relevant reaction kinetics.[3-8]

It has been generally accepted that the cathodic active sites on Mn perovskite/YSZ electrodes are the three-phase boundary (TPB) sites, which are the contact points between the Mn perovskite electrode and YSZ electrolyte.[3-5] Recently, however, some reports have provided a likely evidence whereby the surface oxide vacancies on Mn perovskites also actively participate in the O_2 reduction reaction.[6-8] Undoubtedly, cathode materials having such additional surface reaction sites are highly desirable because, if this is the case, O_2 reduction can take place on the whole electrode surface such that a higher current density can be delivered. One of the major concerns in this study was to check if the surface sites on Mn perovskite electrodes are active for the O_2 reduction reaction. To accomplish this goal, we first measured the oxygen stoichiometry factor (δ) of Mn perovskites at the operating temperature (700-1000 °C) and then examined if the δs have any relation with the cathodic activity of Mn perovskites. Here, it is very likely that if the cathodic activity is not related with δ, the active sites are confined to the TPB sites. By contrast, if the two parameters are related to each other, more specifically, Mn perovskites of lower δs (higher surface oxygen vacancies) exert better activities, it can surely be said that the surface sites are active. The oxygen stoichiometry factor (δ) in Mn perovskites was chemically analyzed and the cathodic activity was estimated by taking steady-state polarization and ac impedance measurements.

Concerning the oxygen reduction kinetics over these electrodes, there also appears a discrepancy in the literatures. Indeed, the oxygen reduction reaction, as it is a four-electron process, can have several elementary steps and almost all the possible elementary steps have been proposed as the limiting step; dissociative adsorption of molecular oxygen on the electrode,[3] diffusion of atomic oxygen over the electrode surface,[4] and the charge transfer reaction.[9] This contradiction is believed to result partly from the differences in electrode morphology and also from the differences in the methods of data analysis. As a way for data analysis, many reports utilized the Butler-Volmer formalism that is commonly used for kinetic study of multi-step, multi-electron electrochemical processes.[10] In some unsuccessful utilization of this formalism, however, a constraint was made for the symmetry factor for the charge transfer step, β=0.5. In this study, we allowed the symmetry factor to be 0.3-0.7 to have a successful data interpretation, which is believed to be more realistic in nature.

Experimentally, steady-state polarization curves and Tafel plots were obtained, from which oxygen reduction kinetics including the rate-determining step were postulated. Ac impedance measurements were also made to get additional information. For this, the P_{O2}-dependent charge transfer resistances (R_{ct}) were measured first, then the exponent m in relation of I_0 (exchange current density $\propto 1/R_{ct}$) $\propto P_{O_2}^m$ was estimated.

Experimentals

Materials. Mn perovskites were prepared according to

the citrate gel method.[8] For this, aqueous solutions of nitrate of La, Sr, and Mn were mixed in a proper molar ratio, into which an excess amount of citric acid (1.2 times of the equivalent) was added. The resulting solution was then concentrated to have a viscous sol and further dried under vacuum to have a gel. The gel was crushed and calcined at 800 °C for 5 hrs. The resulting powder was milled for 12 hrs in ethyl alcohol using zirconia media. The final powder product was obtained after screening through 400 mesh standard sieve. X-ray powder diffraction analysis of the product indicated a perovskite structure with no discernable impurities.

Deposition of Electrodes. The powder was dispersed in turpentine oil and silk-printed (400 mesh) on a YSZ disk (diameter=1.8 cm, thickness=1 mm). Sintering was performed at 1200 °C for 6 hrs. As the counter and reference electrodes, Pt paste (Ferro # 4082) was silk-printed (100 mesh) on the other side of the disk and sintered at 950 °C for 1 hr. The area of the working, counter and reference electrode was 0.22 cm^2, 1.17 cm^2 and 0.15 cm^2, respectively.

For the electrical contact, a piece of Pt gauze was contacted on the cathode surface and pressed with an alumina tube. For the counter and reference electrodes, Pt wires were attached on the electrodes with Pt paste.

Electrochemical Measurements. The cell was placed in a furnace and the oxygen partial pressure was controlled by mixing a proper ratio of nitrogen and oxygen. The actual O_2 pressure was measured with an oxygen sensor prepared with a zirconia tube and Pt paste. The total flow rate was controlled to be 150 cm^3 min^{-1}. Electrochemical measurements were made with a three electrode configuration. Only the half-cell characteristics of the cathode were investigated. The oxygen partial pressure in both sides of the cell was the same. Experiments were performed under 10^{-3}-1 atm of P_{O_2} and the measured temperature was in the range of 700-900 °C.

Ac impedance measurements were made over the frequency range of 0.05 Hz-100 kHz using an EG&G PARC 173 potentiostat, 276 interface, and 5208 two-phase lock-in analyzer. Deconvolution of complex impedance spectra was performed with EG&G PARC 378 electrochemical impedance software. Steady-state polarization measurements were made with the same potentiostat, 175 function generator, and 276 interface. The scan rate was fixed at 0.05 mVs^{-1}.

To analyze the oxygen stoichiometry of electrode materials, first the samples (x=0.1-0.4) were equilibrated at 700-900 °C under P_{O_2}=0.21 atm for 48 hrs, and then the samples were quenched by dropping them into a liquid nitrogen bath. The total Mn content and Mn^{4+} fraction were analyzed by the potentiometric titration method[11] and the Sr and La contents by the ICP (inductively-coupled plasma) method. Oxygen stoichiometric factor (δ) was calculated based on these analytical results.

Results and Discussion

Steady-state polarization measurements. The overall oxygen reduction reaction on SOFC cathodes can be expressed as;

$$O_{2(gas)} + 2V\ddot{o} + 4e' = 2O_O^x \quad (1)$$

where $V\ddot{o}$ and O_O^x represent the doubly-charged oxygen vacancies and lattice oxygen sites, respectively, in Kroger-Vink notation. Here, if the reaction takes place at the TPB sites, the two notations belong to the electrolytes, whereas if it occurs on the electrode surface sites, they represent those on the electrode materials.

Commonly, reaction mechanisms in multi-step, multi-electron transfer processes are analyzed after taking the transfer coefficients in Butler-Volmer equation,[10]

$$I = I_0[\exp(\alpha_a F\eta/RT) - \exp(-\alpha_c F\eta/RT)], \quad (2)$$

with

$$\alpha_c = \vec{\gamma}/\nu + r\beta, \quad (3)$$

$$\alpha_a = (n-\vec{\gamma})/\nu - r\beta, \text{ and} \quad (4)$$

$$\alpha_c + \alpha_a = n/\nu \quad (5)$$

where the notations have their usual meanings.

In this formalism, it is generally assumed that the rate-determining step controls the overall reaction rate and the other elementary steps are facile under equilibrium or quasi-equilibrium. The transfer coefficients (α_c and α_a), which are obtained from Tafel slopes, are the key parameters utilized

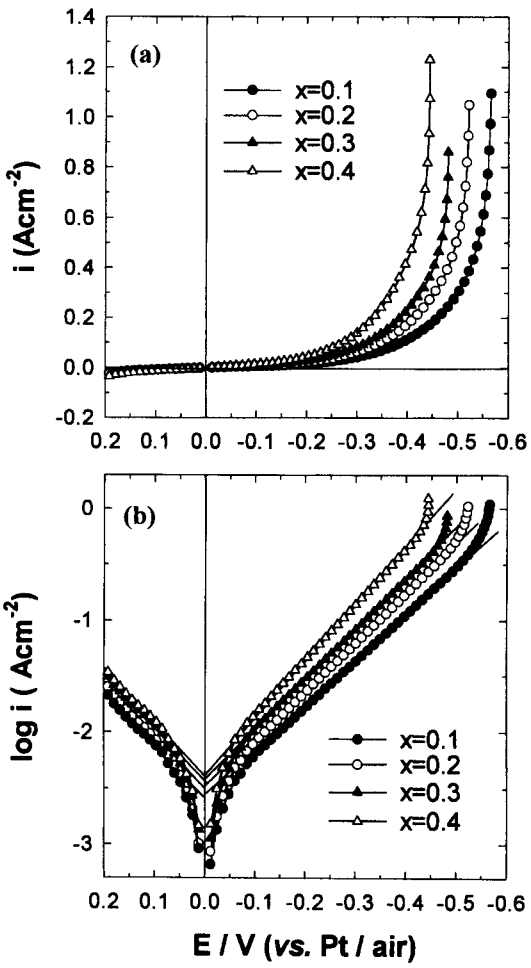

Figure 1. Steady-state polarization curves (a) and corresponding Tafel plots (b) for $La_{1-x}Sr_xMnO_{3+\delta}$/YSZ/Pt cell at 900 °C and Po_2= 0.21 atm.

Table 1. Electrochemical parameters for $La_{1-x}Sr_xMnO_3$ obtained from the steady-state polarization and ac impedance measurements (P_{O_2}=0.21 atm)

Temp (°C)	Sr contents (x)	α_c	α_a	n/ν ($\alpha_a+\alpha_c$)	I_o (Acm^{-2}) (P_{O_2}=0.21 atm)	m in $I_o \propto Po_2^m$ Polarization*	AC impedance*
700	0.1	0.80	1.02	1.82	3.9×10^{-5}	0.280	0.278
	0.2	0.95	0.99	1.94	4.1×10^{-5}	0.255	0.251
	0.3	1.08	0.95	2.03	5.0×10^{-5}	0.234	0.233
	0.4	1.13	0.94	2.07	6.1×10^{-5}	0.227	0.219
800	0.1	0.61	1.20	1.81	2.1×10^{-4}	0.331	0.339
	0.2	0.92	1.01	1.93	2.9×10^{-4}	0.262	0.270
	0.3	1.17	0.82	1.97	3.1×10^{-4}	0.203	0.190
	0.4	1.22	0.81	2.03	4.9×10^{-4}	0.199	0.182
900	0.1	0.52	1.18	1.70	2.1×10^{-3}	0.347	0.349
	0.2	0.94	1.12	2.06	3.2×10^{-3}	0.272	0.272
	0.3	1.27	0.87	2.14	4.0×10^{-3}	0.203	0.177
	0.4	1.36	0.72	2.08	5.1×10^{-3}	0.173	0.132

*Calculated from $m=(1-j)/2$ and $j=\alpha_c/(\alpha_c+\alpha_a)$. **Calculated from the P_{O_2}-dependent R_{ct} measurements.

for the identification of appropriate reaction mechanisms.

Typical steady-state polarization curves and the corresponding Tafel plots are represented in Figure 1, which were obtained with x=0.1-0.4 electrodes at P_{O_2}= 0.21 atm and T=900 °C. Two features are apparent in Figure 1. First of all, there appears no limiting behavior in the i-V profiles, illustrating that the overall reaction is not mass transfer controlled but charge transfer controlled in this potential range. A careful inspection on the Tafel slopes reveals the second characteristics whereby the slopes, thus, the transfer coefficients are Sr-content-dependent. All the observed kinetic data including the anodic and cathodic transfer coefficients are listed in Table 1. The results obtained with the x=0.1 electrode at different oxygen pressure and temperature are tabulated in Table 2. A brief inspection on the listed numbers in Table 1 and 2 illustrates that n/ν ($=\alpha_c+\alpha_a$) is close to 2.0 in the whole measurements, suggesting that the stoichiometric factor ν=2 (*i.e.*, two rds's are involved for the overall reaction) since n=4 in O_2 reduction reaction. This constraint allows only three possible reaction schemes as depicted in Table 3. The three schemes are drawn based on the constraint that the overall kinetics are controlled by the charge transfer step but they are distinguished by the nature of the rate-determining step. As listed in Table 1 and 2, both α_c and α_a are in the range of 0.5-1.4. From this, scheme ***A*** has been excluded since β should have values higher than 1.0 if this is the case. Scheme ***B*** is also discarded with the same argument. Only scheme ***C*** seems to be reasonable because the conditions of $0.5<\alpha_c=2\beta<1.4$ and $0.5<\alpha_a=2\text{-}2\beta<1.4$ fulfill the restriction of $0<\beta<1$. A tentative conclusion is thus made that the two-electron transfer to atomically adsorbed oxygen is the rate-determining step on these electrode materials.

Table 2. Electrochemical parameters obtained from the steady-state polarization measurement for $La_{0.9}Sr_{0.1}MnO_3$

Temp (°C)	Po_2 (atm)	α_c	α_a	n/ν ($\alpha_a+\alpha_c$)	R_{ct}* (Ωcm^2)	R_{ct}** (Ωcm^2)	I_o*** (A/cm^2)
700	0.210	0.80	1.02	1.82	1.2×10^3	1.1×10^3	3.8×10^{-5}
	0.175	0.80	1.01	1.81	1.4×10^3	1.2×10^3	3.5×10^{-5}
	0.104	0.80	1.02	1.82	1.6×10^3	1.6×10^3	2.6×10^{-5}
	0.054	0.81	1.01	1.82	1.9×10^3	1.8×10^3	2.3×10^{-5}
800	0.210	0.61	1.20	1.81	2.8×10^2	2.2×10^2	2.1×10^{-4}
	0.175	0.57	1.18	1.75	3.3×10^2	2.9×10^2	1.6×10^{-4}
	0.104	0.61	1.20	1.81	4.0×10^2	3.1×10^2	1.5×10^{-4}
	0.054	0.62	1.21	1.83	4.8×10^2	3.5×10^2	1.3×10^{-4}
900	0.210	0.52	1.18	1.70	2.9×10^1	2.4×10^1	2.1×10^{-3}
	0.175	0.51	1.17	1.68	3.7×10^1	4.4×10^1	1.1×10^{-3}
	0.104	0.52	1.18	1.71	4.6×10^1	4.8×10^1	1.1×10^{-3}
	0.054	0.54	1.19	1.73	5.7×10^1	5.1×10^1	1.0×10^{-3}

*Calculated from the ac impedance measurements. **Calculated from the linear slopes in steady-state polarization measurements (For example, see Figure 1a). ***Calculated from $I_0=\nu RT/nFR_{ct}$, where ν=2 and n=4.

Table 3. Possible reaction schemes and the resultant transfer coefficients predicted from the Butler-Volmer formalism

A: $2(O_{ad} + V_O^{\cdot\cdot} + e' \rightarrow O_O^{\cdot})$ (rds)
$2(O_O^{\cdot} + e' = O_O^x)$
B: $2(O_{ad} + V_O^{\cdot\cdot} + e' = O_O^{\cdot})$
$2(O_O^{\cdot} + e'\ O_O^x)$ (rds)
C: $2(O_{ad} + V_O^{\cdot\cdot} + 2e'\ O_O^x)$ (rds)

rds	n	r	ν	$\overrightarrow{\gamma}$	$\overleftarrow{\gamma}$	α_c	α_a	$\alpha_c+\alpha_a=n/\nu$
A	4	1	2	0	2	β	2-β	2
B	4	1	2	2	0	1+β	1-β	2
C	4	2	2	0	0	2β	2-2β	2

Relationship of I_o (exchange current density) $\propto$ Po_2^m. If the charge transfer to atomically adsorbed oxygen is rate-controlling, the exchange current density can be expressed as follow.

$$I_0 = |I_{0a}| = nFk^0(1-\theta_{eq})[O_O^x]\exp[\alpha_a F(E_{eq}-E^{0'})/RT] \quad (6)$$

$$I_0 = |I_{0c}| = nFk^0\,\theta_{eq}[\text{Vö}]\exp[-\alpha_c F(E_{eq}-E^{0'})/RT] \quad (7)$$

where k^0 indicates the standard rate constant and θ_{eq} the equilibrium fraction of the adsorption sites occupied by atomic oxygen, respectively. From Eqs. (6), (7), the following expressions are derived.

$$I_0 = nFk^0[\text{Vö}]^{1-j}\,[O_O^x]^j\,\theta_{eq}^{1-j}(1-\theta_{eq})^j \quad (8)$$

$$I_0 \propto \theta_{eq}^{1-j}(1-\theta_{eq})^j \quad (9)$$

where $j=\alpha_c/(\alpha_a+\alpha_c)$, $\alpha_a=(1-j)n/\nu$, and $\alpha_c=j\cdot n/\nu$

Assuming further the adsorption of molecular oxygen follows the Langmuir adsorption isotherm, θ_{eq} can be expressed as follows.

$$O_{2(gas)} + 2V_{ad} = 2O_{ad} \quad (10)$$

$$\theta_{eq}/(1-\theta_{eq}) = (K_{ad}\cdot P_{O_2})^{1/2} \quad (11)$$

where K_{ad} is the adsorption equilibrium constant. Eq. (11) can be simplified under the two limiting conditions:

(1) If $\theta_{eq}\cong 1$, where $K_{ad}\cdot P_{O_2}\gg 1$ which is valid under lower temperature and higher oxygen partial pressure,

$$I_0 \propto P_{O_2}^{-j/2} \quad (12)$$

(2) If $1-\theta_{eq} \simeq 1$, where $K_{ad} \cdot P_{O_2} \ll 1$ which is pertinent at higher temperature and lower oxygen pressure,

$$I_0 \propto P_{O_2}^{(1-j)2} \quad (13)$$

Eq. (12) and (13) illustrates that, regardless of the limiting conditions, the exponent ($-j/2$ or $(1-j)/2$) can be calculated from the α_a and α_c values which can be obtained from the Tafel slopes since $j=\alpha_c/(\alpha_a+\alpha_c)$. Also, since the exponent in Eq. (12) has a negative value whereas it is positive in Eq. (13), the validity between the two limiting conditions can simply be tested from the experimetally observed exponent values (m) in the relation of I_0 ($\propto 1/R_{ct}$) $\propto P_{O_2}^m$.

The m values were assessed from the ac impedance measurements where the charge transfer resistances (R_{ct}) were obtained as a function of oxygen partial pressure. In Figure 2a, typical impedance spectra under different oxygen pressure are represented and one of the deconvoluted spectrum with the equivalent circuit indicated in the inset is displayed in Figure 2b, where three depressed semicircles can be identified. It is apparent in Figure 2a that the size of the lowest frequency arc is strongly dependent on the oxygen pressure, on the other hand, the two higher frequency semicircles are rather invariant. From this, the lowest frequency arc (R_4Q_4) is attributed to the parallel combination of the charge transfer resistance for the O_2 reduction and the CPE (constant phase element),[12,13] whereas the higher frequency semicircles to the grain boundary component in the YSZ (R_2Q_2) and the interfacial product layer ($La_2Zr_2O_7$) formed at the electrolyte/electrode interface region (R_3Q_3).[14,15] The formation of $La_2Zr_2O_7$ at the Mn perovskite/YSZ interface is clearly demonstrated in the XRD pattern (Figure 3) which

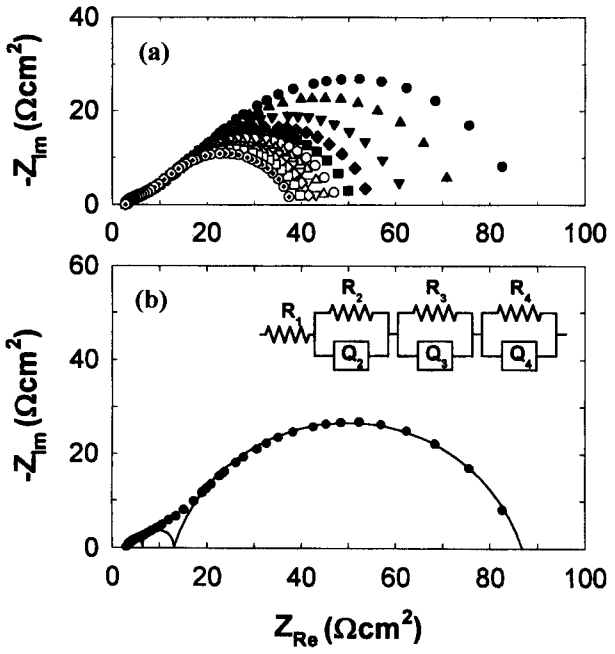

Figure 2. (a); P_{O2}-dependent ac impedance spectra observed with $La_{0.9}Sr_{0.1}MnO_{3+\delta}$/YSZ/Pt cells at 800 °C (●; 0.05 atm, ▲; 0.09 atm, ▼; 0.17 atm, ◆; 0.25 atm, ■; 0.33 atm, ○; 0.41 atm, △; 0.49 atm, ▽; 0.57 atm, ◇; 0.65 atm, □; 0.74 atm and ⊙; 0.95 atm, and (b); equivalent circuit and deconvoluted spectrum for the data of P_{O_2}=0.05 atm.

was taken after the electrode layer being removed from the YSZ surface. Figure 3 shows an appearance of the diffraction peaks belonging to $La_2Zr_2O_7$. In the meantime, the R_1 corresponds to the electrolyte resistance between the cathode and reference electrode.

Typical log ($1/R_{ct}$) *vs.* log P_{O_2} plots are represented in Figure 4, where the exponent m in I_0 ($\propto 1/R_{ct}$) $\propto P_{O_2}^m$ is indicated. The m values obtained from the ac impedance analysis are listed in the last column of Table 1. The numbers are in the range of 0.13-0.35, but more importantly, they are positive, illustrating that the O_2 reduction reaction rate is faster at higher O_2 pressure. The positive m also suggests that the limiting condition pertinent to Eq. (13), that is, a high temperature and low oxygen pressure regime, is valid in the present measurements since $j=\alpha_c/(\alpha_a+\alpha_c)$ is positive. The exponents, $(1-j)/2$ as in Eq. (13), were thus calculated from the α_a and α_c and they are listed in the second last column in Table 1. A comparison of two sets of m in Table 1, one calculated from the steady-state polarization meas-

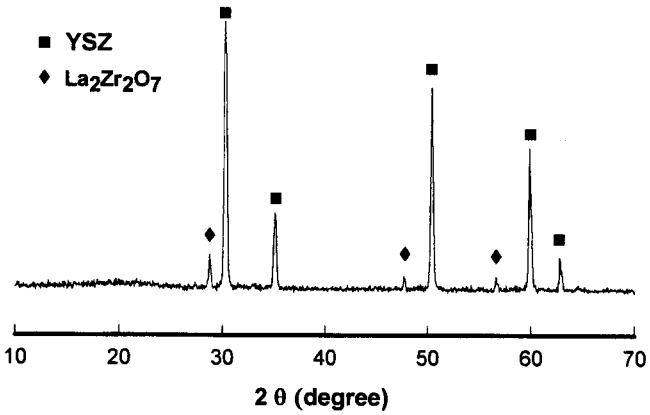

Figure 3. XRD patterns traced on the $La_{0.9}Sr_{0.1}MnO_{3+\delta}$/YSZ interface region. The electrode layer was removed after cell operation.

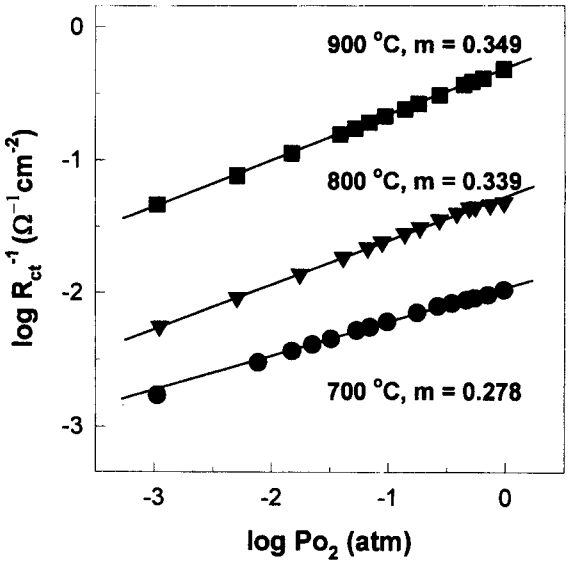

Figure 4. Log ($1/R_{ct}$) *vs.* log P_{O_2} plots for $La_{0.9}Sr_{0.1}MnO_{3+\delta}$/YSZ/Pt cells at different temperature. The slopes (m) are indicated.

urements using Eq. (13) and the other from the ac impedance measurements, shows that they are matched well within experimental errors. In the meantime, Table 2 also compares the R_{ct} obtained from the two measurements. Note that the two measurements are well-matched with each other. This consistency in m and R_{ct} between the two measurements not only demonstrates the accuracy of the measurements and the correctness in data interpretation, but enables us to draw a conclusion that the rate-determining step for O_2 reduction on the manganites is the charge transfer process to the atomic oxygen and the present experimental conditions belong to a higher temperature and lower oxygen pressure regime.

Relationship between transfer coefficients (α_a and α_c) and oxygen stoichiometry factor (δ) of Mn perovskites. It is known that the oxygen stoichiometry factor in $LaMnO_{3+\delta}$ is originated from the following intrinsic defect reaction,[16]

$$6Mn_{Mn}^{x} + 3/2O_2 = 3O_o^{x} + V_{La}''' + V_{Mn}''' + 6Mn_{Mn}^{\cdot} \quad (14)$$

When the La^{3+} ions are partially replaced by Sr^{2+} ions, additional extrinsic defects are created as follows.

$$[Sr_{La}'] = [Mn_{Mn}^{\cdot}] \quad (15)$$

Therefore, if Mn perovskites contain both the intrinsic and extrinsic defects, the oxygen stoichiometric factor and metal vacancy fractions are expressed as follows.[16]

$$\frac{\delta}{3} = [V_{La}'''] = [V_{Mn}'''] = K_{V_M}^{1/2}\frac{(1-[Sr_{La}'])^3}{[Sr_{La}']^3}P_{O_2}^{3/4} \quad (16)$$

Here, K_{V_M}' represents the equilibrium constant for the reaction (14). Eq. (16) indicates that δ are determined by the K_{V_M}, Sr-doping contents and oxygen pressure. The K_{V_M} is known to decrease with an increasing temperature such that δ becomes smaller at higher temperature.[17] Also, Eq. (16) suggests that δ becomes smaller with Sr-doping. Figure 5 displays the oxygen stoichiometry factors as a function of Sr-doping contents and temperature. In this measurement, P_{O_2} was fixed at 0.21 atm. As expected from Eq. (16), the δ decrease with an increase in temperature and Sr-doping.

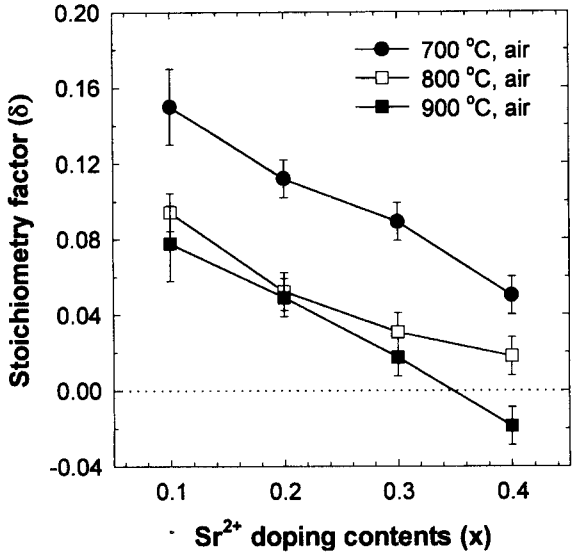

Figure 5. Oxygen stoichiometry factor (δ) of $La_{1-x}Sr_xMnO_{3+\delta}$ as a function of Sr-doping contents and temperature. P_{O_2}=0.21 atm.

In order to see the relation between the cathodic activities of Mn perovskites and their oxygen stoichiometry factors, the α_a and α_c that were observed with $La_{1-x}Sr_xMnO_{3+\delta}$ (x= 0.1-0.4) at 700-900 °C and P_{O_2}=0.21 atm are plotted against δ (Figure 6). It can be seen that the cathodic transfer coefficient decreases with an increasing oxygen stoichiometry factor, whereas the anodic one shows the reverse trend. These results manifest themselves that the O_2 reduction reaction becomes more favorable if the electrode materials have more oxide vacancies, but in turn the reverse reaction, the electrochemical oxidation of oxide ion to molecular oxygen, becomes slower.

Two types of active reaction sites for O_2 reduction have been proposed in the manganite electrodes; the oxide vacancy sites on the electrode surface and three-phase boundary sites. The results presented so far favor the former possibility because the cathodic transfer coefficients become larger on the Mn perovskites having lower oxygen stoichiometry. However, in view of the fact that the oxygen stoichiometry factor is positive, that is, the electrodes show oxygen overstoichiometry, the oxide bulk diffusion would not be so high that oxide ions, even if they are produced on the electrode surface, are difficult to migrate to the electrolyte. Rather, surface or grain boundary diffusion of oxide ions is more likely to occur.

The cathodic transfer coefficient (α_c) steadily increases with Sr-doping contents as can be seen in Figure 7. As higher α_c is favorable for O_2 reduction, the x=0.4 electrode would be the best choice among the tested materials. In the meantime, we found that the cathodic activities of heavily doped Mn perovskites (x>0.5) are worse than the x=0.4 electrode. A plausible explanation for this can not be given

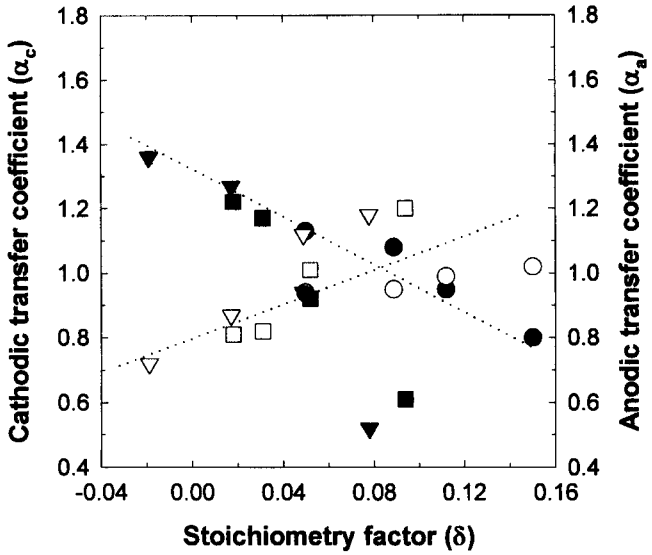

Figure 6. Transfer coefficients (α_c and α_a) *vs.* oxygen stoichiometry factor (δ). The results were obtained with $La_{1-x}Sr_xMnO_{3+\delta}$ (x=0.1-0.4) at 700-900 °C and P_{O_2}=0.21 atm. α_c values: ●; 700 °C, ■; 800 °C, ▼; 900 °C and α_a values: ○; 700 °C, □; 800 °C, ▽; 900 °C.

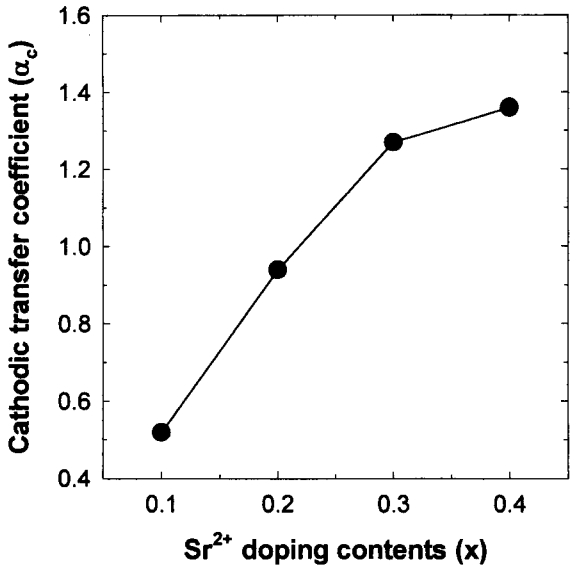

Figure 7. Cathodic transfer coefficients (α_c) for O_2 reduction reaction according to the Sr-doping contents for $La_{1-x}Sr_xMnO_{3+\delta}$/YSZ/Pt cells observed at 900 °C in air.

at this moment. But it should be noted that the high temperature phase stability of Mn perovskites becomes poorer as the Sr-doping content becomes higher.

Conclusion

In this report, we presented the results of O_2 reduction kinetics and active reaction sites in Mn perovskite electrodes. The steady-state polarization and ac impedance measurements were carried out to extract a unified view on O_2 reduction kinetics. In addition, a comparison of results on the oxygen stoichiometry factors of Mn perovskites and their cathodic activities allows us to locate the active reaction sites for O_2 reduction. Some valuable points are in order:

(i) Combined results from the steady-state polarization and ac impedance measurements suggest that the slowest step in the overall O_2 reduction on $La_{1-x}Sr_xMnO_{3+\delta}$ (x=0.1-0.4) is the charge transfer process to atomically adsorbed oxygen. The calculated exponents m in $I_o \alpha P_{O_2}^m$ from the steady-state polarization are well matched with those obtained from the P_{O_2} dependent ac impedance measurements.

(ii) There is an inverse relationship between the cathodic transfer coefficients (α_c) of O_2 reduction and the oxygen stoichiometry factor (δ) of Mn perovskites, reflecting that surface oxide vacancies are actively involved in the oxygen reduction reaction.

(iii) Among those Mn perovskite electrode materials (x= 0.1-0.4), the x=0.4 sample shows the lowest oxygen stoichiometry factor and consistently it gives the highest α_c and the best cathodic activity.

Acknowledgment. We are grateful to the Korea Science and Engineering Foundation for supporting this work.

References

1. Murugesamoorthi, K. A.; Srinivasan, S.; Appleby, A. J. *Fuel Cell Systems*; Blomen, L. J. M. J.; Mugerwa, M. N. Eds. Plenum Press: New York, 1993; pp 464-473.
2. Hammou, A. *Advances in Electrochemical Science and Engineering*; Gerischer, H.; Tobias, C. W. Eds. VCH Publishers: New York, 1992; pp 87-140.
3. Takeda, Y.; Kanno, R.; Noda, M.; Tomida, Y.; Yamamoto, O. *J. Electrochem. Soc.* **1987**, *134*, 2656.
4. Mizusaki, J.; Tagawa, H.; Tsuneyoshi, K.; Sawata, A. *J. Electrochem. Soc.* **1991**, *138*, 1867.
5. de Haart, L. G. J.; Kuipers, R. A.; de Vries, K. J.; Burggraaf, A. J. *J. Electrochem. Soc.* **1991**, *138*, 1970.
6. Hammouche, A.; Siebert, E.; Hammou, A. *Mater. Res. Bull.* **1989**, *24*, 367.
7. Hammouche, A.; Siebert, E.; Hammou, A.; Kleitz, M.; Caneiro, A. *J. Electrochem. Soc.* **1991**, *138*, 1212.
8. Lee, H. Y.; Cho, W. S.; Oh, S. M.; Wiemhöfer, H.-D.; Göpel, W. *J. Electrochem. Soc.* **1995**, *142*, 2659.
9. Inoue, T.; Seki, N.; Eguchi, K.; Arai, H. *J. Electrochem. Soc.* **1990**, *137*, 2523.
10. O'M Bockris, J.; Reddy, A. K. N. *Modern Electrochemistry*, Vol. 2; Plenum Press: New York, 1973; p 999.
11. Jeffery, G. H.; Bassett, J.; Mendham, J.; Denney, R. C. *Vogel's Textbook of Quantitative Chemical Analysis*; Longman Scientific & Technical: UK, 1989; p 375.
12. Van Hassel, B. A.; Boukamp, B. A.; Burggraaf, A. J. *Solid State Ionics* **1991**, *48*, 155.
13. Macdonald, J. R. *Impedance spectroscopy emphasizing solid materials and systems*; John Wiley & Sons: New York, 1987; p 13.
14. Lee, H. Y.; Oh, S. M. *Solid State Ionics* **1996**, *90*, 133.
15. Yokogawa, H.; Sakai, N.; Kawada, T.; Dokiya, M. *Solid State Ionics* **1990**, *40/41*, 398.
16. Kofstad, P.; Petrov, A. *High Temperature Electrochemical Behaviour of Fast Ion and Mixed Conductors*; Risφ National Laboratory: Roskilde, Denmark, 1993; p 287.
17. Kuo, J. H.; Anderson, H. U.; Sparlin, D. M. *J. Solid State Chem.* **1989**, *83*, 52.